

# A V-Shaped PM Vernier Motor With Enhanced Flux-Modulated Effect and Low Torque Ripple

Yiqiang Chen, Xiaoyong Zhu<sup>1b</sup>, Li Quan, Zixuan Xiang, Yi Du<sup>1b</sup>, and Xiaoxiao Bu

School of Electrical and Information Engineering, Jiangsu University, Zhenjiang 212013, China

This paper proposes a new V-shaped permanent magnet vernier (V-PMV) motor for potential applications in direct-drive system. By utilizing the V-shaped PM topology and suitable pole-slot ratio, not only the flux leakage can be reduced effectively which is inevitable in traditional surface-mounted and spoke-type vernier permanent magnet (VPM) motor, but also the utilization of air-gap magnetic field harmonics can be improved. Moreover, dummy slots are employed on the inner edge of rotor, so that the torque ripple can be reduced. To fairly estimate electromagnetic performances of the proposed V-PMV motor, an existing flux-concentrating VPM motor is selected purposely and designed with the same size for comparative analysis by using the finite-element method. The simulation results indicate that the V-PMV motor can offer the advantages of high PM utilization, and low cogging torque and torque ripple.

*Index Terms*—Direct drive, flux-modulated effect, torque ripple, vernier motor.

## I. INTRODUCTION

VERNIER permanent magnet (VPM) motors have attracted more and more interest and attention, which have been considered as one of the promising candidates for direct-drive applications, such as electric vehicles and wind power generation [1], [2]. As one of the new type of flux-modulated motors, VPM motors have abundant harmonic components in air-gap magnetic field, thus possessing the advantage of high torque density.

Recently, many various VPM motor topologies were proposed and investigated, such as the surface-mounted VPM motor and spoke-type VPM motor [3], [4]. However, the inevitable internal and external flux leakages in abovementioned VPM motors lead to the low PM utilization, especially in VPM motors with spoke-type PM rotor. More importantly, in [5], the fundamental and high-speed harmonics in air-gap magnetic field are usually taken into consideration, while the low-speed harmonics are neglected. However, abundant low-speed harmonics with high amplitude exist in air-gap magnetic field, so the torque capability can be enhanced effectively by utilizing these low-speed harmonics, which offers a new path for further improving the torque density of VPM motors. Hence, how to design a VPM motor with high torque density by taking full advantage of the low-speed harmonics is becoming a hot issue and research orientation in motor filed.

In this paper, based on the design concept of flux modulation [6], [7], a V-shaped permanent magnet vernier (V-PMV) motor is proposed, where not only the fundamental and high-speed harmonic components contribute to the torque output, but also low-speed harmonics with high amplitude are utilized to improve its torque further. Moreover, by adopting the V-shaped PM topology and dummy slots in rotor, the flux leakage can be reduced and the pole-arc coefficient of rotor can be adjusted to provide a possibility for achieving both high torque density and low torque ripple.

Manuscript received March 8, 2018; revised April 12, 2018; accepted April 14, 2018. Corresponding author: X. Zhu (e-mail: zxyff@ujs.edu.cn).

Color versions of one or more of the figures in this paper are available online at <http://ieeexplore.ieee.org>.

Digital Object Identifier 10.1109/TMAG.2018.2828989

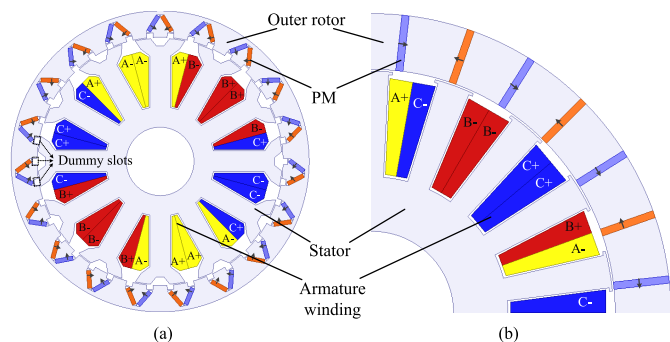


Fig. 1. Motor configurations. (a) Proposed V-PMV motor. (b) FC-VPM motor.

## II. MOTOR DESIGN AND OPERATING PRINCIPLE

### A. Topology Design of Motor

Fig. 1(a) shows the proposed V-PMV motor. Compared with the existing flux-concentrating (FC) VPM shown in Fig. 1(b), the rotor with V-shaped PM topology can avoid the external flux leakages and reduce internal flux leakages, thus improving the PM utilization as well as the output torque. And the V-shaped PM arrangement of the proposed motor rotor can enable the PMs withstand more compressive stress and less tensile stress to avoid the damage and shedding in the rotating rotor, so that the mechanical strength of the motor can be increased. In addition, dummy slots with the same number of PMs are arranged on inner edge of rotor to achieve an adjustable pole-arc coefficient, thus performing the decrease of torque ripple. Furthermore, the proposed motor uses the split-slot design, which aims at enhancing the flux-modulated effect by designing suitable stator/rotor pole combination. To evaluate the advantages of the proposed V-PMV motor, an FC-VPM motor [4] is selected purposely and designed with the same overall dimension for fair comparative analysis.

### B. Operating Principle

According to the principle of coaxial magnetic gear [8], [9], a series of flux density space harmonics will occur in the air gap due to the modulation function of modulating poles to magnetic field produced by the PMs. And the pole-pair

number (PPN) of these harmonics can be expressed as

$$P_{m,n} = |mP_{pm} + nN_{ss}| \quad (m = 1, 3, 5, \dots, \infty; n = 0, \pm 1, \pm 2, \pm 3, \dots, \pm \infty). \quad (1)$$

The rotation speeds of these flux density space harmonics can be given by

$$\omega_{m,n} = \frac{mP_{pm}}{mP_{pm} + nN_{ss}}\omega_{PM} + \frac{nN_{ss}}{mP_{pm} + nN_{ss}}\omega_{ss} \quad (2)$$

where  $P_{pm}$  is the PPN of PM,  $N_{ss}$  is the number of flux modulating poles, and  $\omega_{pm}$  and  $\omega_{ss}$  are the rotation speeds of PMs and flux modulating poles, respectively. When the PMs are located on the rotor, the stator salient teeth play the role of flux modulating poles in VPM motors. So  $N_{ss}$  is the number of stator salient teeth and  $\omega_{ss} = 0$ . When the proposed motor adopts split-slot stator, each stator tooth has two modulating poles in this paper, and  $N_{ss}$  is twice of the stator slot number  $N_s$ . So the PPN and rotation speeds of the flux density space harmonics in rotor PM motor can be redefined as

$$P_{m,n} = |mP_{pm} + nN_{ss}| = |mP_{pm} + 2nN_s| \quad (m = 1, 3, 5, \dots, \infty; n = 0, \pm 1, \pm 2, \pm 3, \dots, \pm \infty) \quad (3)$$

$$\omega_{m,n} = \frac{mP_{pm}}{mP_{pm} + nN_{ss}}\omega_{PM} = \frac{mP_{pm}}{mP_{pm} + 2nN_s}\omega_{PM}. \quad (4)$$

It can be seen that the combination of  $m = 1$  and  $n = -1$  results in a harmonic with the highest rotation speed  $\omega_{1,-1}$  and the lowest pole pairs, which is defined as high-speed harmonic. And the combination of  $m = 1$  and  $n = 0$  results in a harmonic defined as fundamental harmonic in this paper with the highest amplitude, of which the rotational angular velocity  $\omega_{1,0}$  is the same with that of the rotor. The speed ratio  $G_{m,n}$  that other harmonics to fundamental harmonic is expressed as

$$G_{m,n} = \frac{\omega_{m,n}}{\omega_{1,0}} = \frac{mP_{pm}}{|mP_{pm} + 2nN_s|}. \quad (5)$$

Furthermore, the harmonics except high-speed harmonic and fundamental harmonic are named as low-speed harmonic, of which the pole-pair and rotation speed are decided by different values of  $m$  and  $n$ . So the air-gap flux density  $B_{fd}$  in the proposed V-PMV motor can be expressed as

$$B_{fd}(\theta, t) = \underbrace{B_{1,-1} \cos[p_{1,-1}(\theta - G_{1,-1}\omega_{1,0}t)] + B_{1,0} \cos[p_{1,0}(\theta - \omega_{1,0}t)]}_{\text{High-speed harmonic produced because of field modulation}} + \underbrace{B_{m,n} \cos[p_{m,n}(\theta - G_{m,n}\omega_{1,0}t)]}_{\text{Fundamental harmonic produced by rotor magnets}} + \underbrace{B_{m,n} \cos[p_{m,n}(\theta - G_{m,n}\omega_{1,0}t)]}_{\text{Low-speed harmonic produced because of field modulation}} \quad (6)$$

where  $\theta$  is the circumferential position and  $B_{m,n}$  is the amplitude of the corresponding air-gap flux density space harmonic.

In order to achieve a stable operation of the VPM motor, the armature windings need to be wound according to the working harmonics in the air gap. And the electrical degree  $\alpha$  between any two adjacent coil electromotive force (EMF) vectors can be determined as [10]

$$\alpha_{P_{m,n}} = \text{sign}(\omega_{m,n}) \times \left( \frac{P_{m,n}}{N_s} - \left[ \frac{P_{m,n}}{N_s} \right] \right) \times 360^\circ. \quad (7)$$

TABLE I  
HARMONIC SPECTRUM COMPARISONS

Items	Proposed V-PMV motor				
	$N_{ss}-P_{pm}$	$P_{pm}$	$2N_{ss}-P_{pm}$	$P_{pm}+N_{ss}$	
Main harmonic order	5	19	29	43	
Amplitude	0.341	1.019	0.344	0.201	
Electrical degree $\alpha$	-150°	210°	-150°	210°	
If utilized (Y/N)	Y	Y	Y	Y	
Winding factor $k_w$	0.933	0.388	0.268	0.175	
Items	FC-VPM motor				
	$N_{ss}-P_{pm}$	$P_{pm}$	$3P_{pm}-N_{ss}$	$3P_{pm}$	$5P_{pm}$
Main harmonic order	4	14	24	32	42
Amplitude	0.267	0.931	0.251	0.547	0.447
Electrical degree $\alpha$	-80°	280°	120°	280°	120°
If utilized (Y/N)	Y	Y	N	Y	N
Winding factor $k_w$	0.945	0.416	\	0.187	\

It is known that the coil-EMF vectors of high-speed harmonic and fundamental harmonic are the same. This can prove that the VPM motor can utilize both the high-speed harmonic and fundamental harmonic in air-gap magnetic field. Hence, in order to obtain better performance, it is necessary to ensure that the amplitudes of high-speed harmonic and fundamental harmonic are relatively higher.

At the same time, in order to obtain high PM utilization and torque density, the low-speed harmonic with high amplitude should be used as much as possible. Hence, for making a clear analysis and comparison of the use of main harmonics in air-gap magnetic field, the corresponding harmonic spectrum analysis results of the proposed V-PMV and FC-VPM motors are obtained by the finite-element method and listed in Table I. It can be found that the low-speed harmonics with high amplitude can be fully utilized in the proposed V-PMV motor, but the 24th and 42th harmonics cannot be used in the FC-VPM motor.

### III. KEY PARAMETER OPTIMIZATION OF MOTOR

For obtaining optimal motor performances of the V-PMV motor, the influences of some key design parameters are investigated and the corresponding parametric model is shown in Fig. 2(a). Considering the potential applications in direct drive, the proposed V-PMV motor requires the performances of high output torque and low torque ripple. Therefore, the output torque and torque ripple are preferred to be selected as the optimization objectives.

Because the configuration of the V-PMV motor is relatively complex, the corresponding number of design variables is relatively large and the influences of each design variable on the optimization objectives are generally different. In order to recognize the influences of each design variable on the optimization objectives effectively, an effective method of comprehensive sensitivity analysis is adopted in this section [11], [12], in which the sensitivity index  $S(y_i)$  is introduced as

$$S(y_i) = \frac{V(E(f(y_i)/y_i))}{V(f(y_i))} \quad (8)$$

where  $f(y_i)$  is the optimization objective,  $E(f(y_i)/y_i)$  is the average value of  $f(y_i)$  when  $y_i$  is constant,  $V(E(f(y_i)/y_i))$  is the variance of  $E(f(y_i)/y_i)$ , and  $V(f(y_i))$  is the variance of  $f(y_i)$ . According to (8), the sensitivity indices of the design variables to the output torque and torque ripple are evaluated and the results are shown in Fig. 2(b). Generally, the high sensitivity index implies a high effect on optimization objective. The positive sensitivity index indicates that the

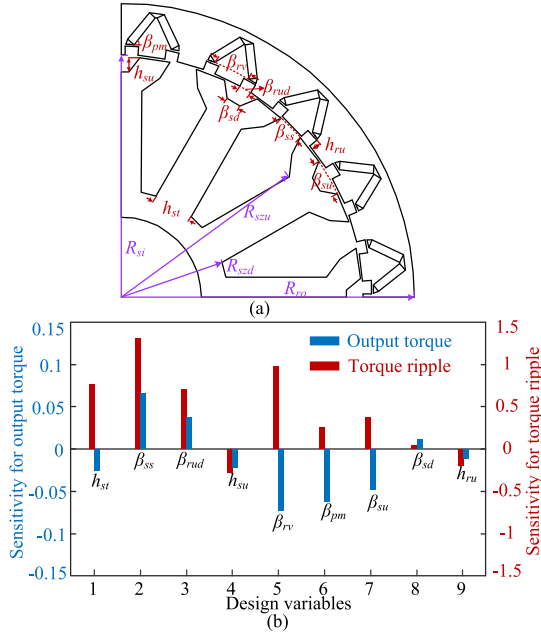


Fig. 2. Parametric model and sensitivity of the proposed V-PMV motor. (a) Parametric model of the proposed V-PMV motor. (b) Results of sensitivity indices of design variables to two optimization objectives.

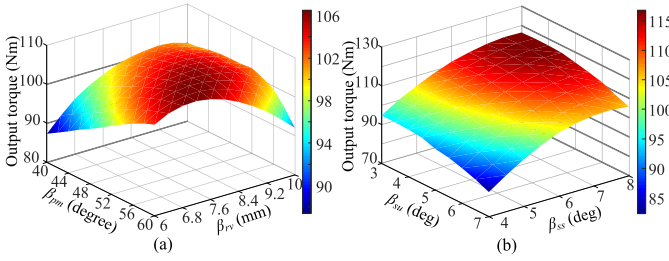


Fig. 3. Response of the proposed V-PMV motor. (a) Output torque distribution between  $\beta_{pm}$  and  $\beta_{rv}$ . (b) Output torque distribution between  $\beta_{ss}$  and  $\beta_{su}$ .

optimization objective will increase with the growth of design variable, while the negative one means a contrary variation. Therefore, it can be seen from Fig. 2(b) that  $\beta_{pm}$ ,  $\beta_{ss}$ ,  $\beta_{su}$ , and  $\beta_{rv}$  have more significant effects for output torque and  $\beta_{ss}$ ,  $\beta_{rv}$ ,  $\beta_{rud}$ , and  $h_{st}$  have more significant effects for torque ripple compared with the remaining design variables. So, these parameters with significant effects for output torque and torque ripple are selected to be investigated, respectively, in Section IV.

#### IV. PERFORMANCE ANALYSIS AND COMPARISON

In this section, by using the finite-element method, the optimization performance of the proposed V-PMV motor and the electromagnetic performances of the FC-VPM and V-PMV motors are investigated. It is noted that these two motors have the same rated speed, current density, motor outer diameter, stack length, air-gap length, and PM volume.

##### A. Optimization Performance of V-PMV Motor

Fig. 3 shows the corresponding relationship of output torque with respect to the significant design variables of  $\beta_{pm}$ ,  $\beta_{ss}$ ,  $\beta_{su}$ , and  $\beta_{rv}$ . It can be seen that with the increase of  $\beta_{pm}$  and  $\beta_{rv}$ , the output torque increases first and then decreases. On the other hand, the output torque increases with the increase of  $\beta_{ss}$  and  $\beta_{su}$ . Fig. 4 shows the corresponding relationship of torque ripple with respect to the significant

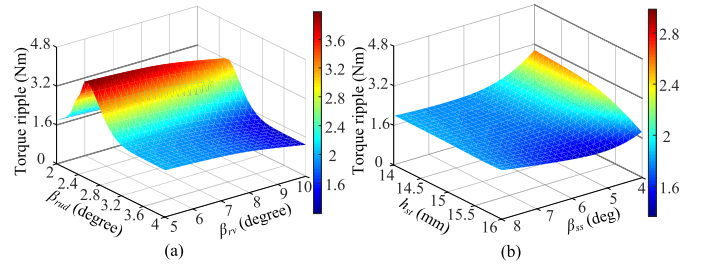


Fig. 4. Response of the proposed V-PMV motor. (a) Torque ripple distribution between  $\beta_{rud}$  and  $\beta_{rv}$ . (b) Torque ripple distribution between  $\beta_{ss}$  and  $h_{st}$ .

TABLE II  
SPECIFICATIONS OF THE TWO MOTORS

Items	V-PMV motor	FC-VPM motor
Stack length $l_a$ (mm)	60	60
Motor outer diameter (mm)	220	220
Motor inner diameter (mm)	60	60
Airgap length (mm)	0.5	0.5
Phase number	3	3
No. of rotor pole-pairs	19	14
No. of stator slots	12	18
No. of flux-modulation pieces	24	18

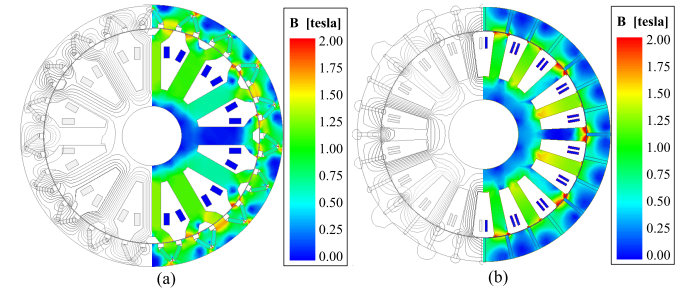


Fig. 5. No-load field and flux density distribution. (a) Proposed V-PMV motor. (b) FC-VPM motor.

design variables of  $\beta_{rud}$ ,  $\beta_{rv}$ ,  $h_{st}$ , and  $\beta_{ss}$ . It can be seen that with the increase of  $\beta_{rud}$ , the torque ripple increases first and then decreases. On the other hand, the torque ripple decreases with the increase of  $h_{st}$ . Hence, considering a compromise between the average torque and torque ripple, the optimal values of design variables are determined. Then, the specific design parameters of the two motors are listed in Table II.

##### B. Basic No-Load Characteristics

Fig. 5(a) and (b) depicts the no-load magnetic field and flux density distributions of the two motors. It can be found that, as expected, the external flux leakage is avoided in the proposed V-PMV motor. At the same time, the average magnetic flux density in stator teeth of the proposed motor is lower than that of the FC-VPM motor. It indicates that the proposed V-PMV motor has a relatively low magnetic saturation.

The no-load air-gap flux density curves of the V-PMV motor and FC-VPM motor are calculated and compared in Fig. 6(a). It can be seen that the peak value of air-gap flux density in the V-PMV motor is 1.7 T, while that of the FC-VPM motor reaches 1.9 T. It agrees with the results from Fig. 5(a) and (b). The corresponding harmonic spectrum analysis of air-gap flux density is given in Fig. 6(b). Obviously, under the same volume of PM, the amplitudes of the fundamental and high-speed harmonics of V-PMV motor are higher than those of the FC-VPM motor. Furthermore, from Fig. 6(b) and Table I, it can be found that the low-speed harmonics with high amplitude are utilized in the V-PMV motor, but the low-speed

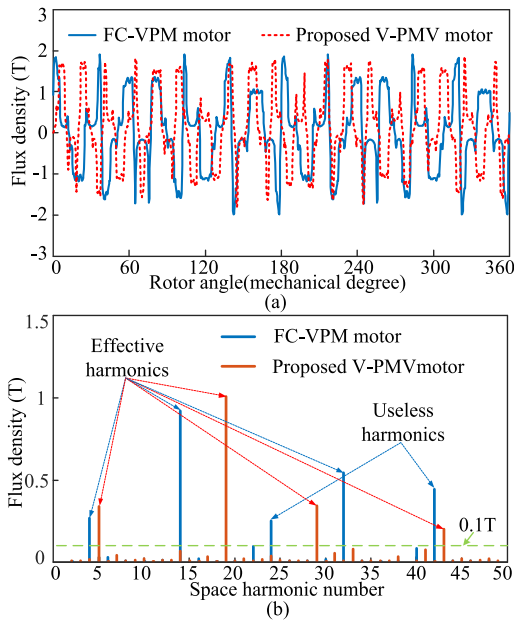


Fig. 6. No-load air-gap flux density. (a) Waveforms. (b) Spectra.

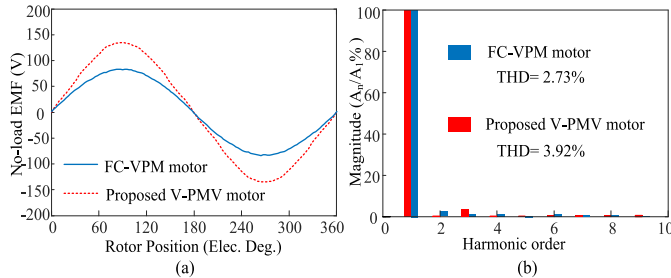


Fig. 7. Back EMF comparison. (a) Waveforms. (b) Spectra.

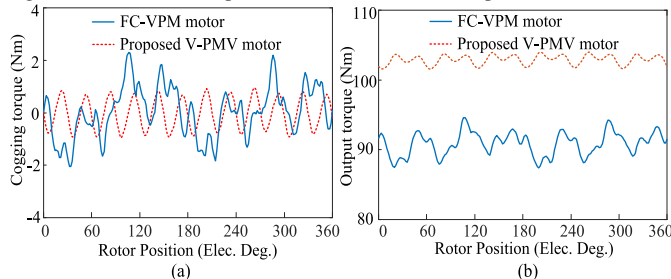


Fig. 8. Torque comparison. (a) Cogging torque. (b) Output torque.

harmonics with the orders of 24th and 42th are not used in the FC-VPM motor. It means that the PM utilization is improved effectively in the V-PMV motor.

### C. Back EMF

Then, the no-load back EMF of two motors is calculated. As shown in Fig. 7(a), both motors possess a symmetrical and sinusoidal back EMF waveforms, and the back EMF amplitude of the proposed motor is higher than that of the FC-VPM motor. As shown in Fig. 7(b), both motors have low total harmonic distortion which is less than 4%. Hence, the brushless ac control can be applied to both motors to obtain high driving performances.

### D. Torque Characteristics

The comparison results of cogging torque and output torque between two motors are shown in Fig. 8(a) and (b), respectively. It can be observed that the peak-to-peak cogging torque

in the proposed V-PMV motor is about  $1.7 \text{ N} \cdot \text{m}$ , which is lower than  $4.3 \text{ N} \cdot \text{m}$  in the FC-VPM motor, and the average torque of the V-PMV motor is  $102.9 \text{ N} \cdot \text{m}$ , which is about 15.2% higher than that of the FC-VPM motor. Meanwhile, the torque ripple of the proposed design is only about 35.2% of the FC-VPM motor, achieving the small value of 0.021. It can be found that the PM utilization is improved effectively by an enhanced flux-modulated effect in the V-PMV motor.

## V. CONCLUSION

This paper proposes a V-PMV motor which not only can utilize both the fundamental and high-speed harmonics in the air-gap flux density, but also the low-speed harmonics with high amplitude can be fully utilized. And by utilizing the V-shaped PM topology in rotor, the flux leakage phenomenon can be avoided effectively. Compared with the FC-VPM motor with the same overall dimensions, the proposed V-PMV motor can not only provide higher PM utilization and torque density, but also possess lower cogging torque and torque ripple, which is preferred to be an interesting candidate in direct-drive applications.

## ACKNOWLEDGMENT

This work was supported in part by the National Natural Science Foundation of China under Grant 51477069 and Grant 51777089 and in part by the Priority Academic Program Development of Jiangsu Higher Education Institutions.

## REFERENCES

- [1] H. Wang *et al.*, "A novel consequent-pole hybrid excited Vernier machine," *IEEE Trans. Magn.*, vol. 53, no. 11, Nov. 2017, Art. no. 8112304.
- [2] D. Li, R. Qu, and T. Lipo, "High-power-factor Vernier permanent-magnet machines," *IEEE Trans. Ind. Appl.*, vol. 50, no. 6, pp. 3664–3674, Nov./Dec. 2014.
- [3] D. Jang and J. Chang, "Effects of flux modulation poles on the radial magnetic forces in surface-mounted permanent-magnet vernier machines," *IEEE Trans. Magn.*, vol. 53, no. 6, Jun. 2017, Art. no. 8202704.
- [4] X. Li, K. T. Chau, and M. Cheng, "Comparative analysis and experimental verification of an effective permanent-magnet Vernier machine," *IEEE Trans. Magn.*, vol. 51, no. 7, Jul. 2015, Art. no. 8203009.
- [5] S. Niu, S. L. Ho, and W. N. Fu, "A novel stator and rotor dual PM Vernier motor with space vector pulse width modulation," *IEEE Trans. Magn.*, vol. 50, no. 2, pp. 805–808, Feb. 2014.
- [6] M. Cheng, P. Han, and W. Hua, "General airgap field modulation theory for electrical machines," *IEEE Trans. Ind. Electron.*, vol. 64, no. 8, pp. 6063–6074, Aug. 2017.
- [7] D. Wang, D. Zhang, X. Du, and X. Wang, "Thermal identification, model, and experimental validation of a toroidally wound mover linear-switched reluctance machine," *IEEE Trans. Magn.*, vol. 54, no. 3, Mar. 2018, Art. no. 8102905.
- [8] H. Shin and J. Chang, "Comparison of radial force at modulating pieces in coaxial magnetic gear and magnetic geared machine," *IEEE Trans. Magn.*, vol. 54, no. 3, Mar. 2018, Art. no. 8101904.
- [9] X. Zhu, Z. Xiang, L. Quan, Y. Chen, and L. Mo, "Multi-mode optimization research on a multi-port magnetic planetary gear permanent magnet machine for hybrid electric vehicles," *IEEE Trans. Ind. Electron.*, to be published, doi: [10.1109/TIE.2018.2813966](https://doi.org/10.1109/TIE.2018.2813966).
- [10] Y. Shi, L. Jian, J. Wei, Z. Shao, W. Li, and C. C. Chan, "A new perspective on the operating principle of flux-switching permanent-magnet machines," *IEEE Trans. Ind. Electron.*, vol. 63, no. 3, pp. 1425–1437, Mar. 2016.
- [11] X. Zhu, Z. Xiang, L. Quan, W. Wu, and Y. Du, "Multimode optimization design methodology for a flux-controllable stator permanent magnet memory motor considering driving cycles," *IEEE Trans. Ind. Electron.*, vol. 65, no. 7, pp. 5353–5366, Jul. 2018.
- [12] Z. Xiang, X. Zhu, L. Quan, Y. Du, C. Zhang, and D. Fan, "Multilevel design optimization and operation of a brushless double mechanical port flux-switching permanent-magnet motor," *IEEE Trans. Ind. Electron.*, vol. 63, no. 10, pp. 6042–6054, Oct. 2016.